

# A Comparison of Acoustic Emission and Vibration Measurements for Condition Monitoring of an Offshore Drilling Machine

Martin Hemmer<sup>1</sup>, Tor I. Waag<sup>2</sup>

<sup>1</sup> Faculty of Engineering and Science, University of Agder, Jon Lilletuns Vei 9, N-4879 Grimstad, Norway

*martin.hemmer@uia.no*

<sup>2</sup> Teknova AS, Tordenskjolds gate 9, N-4612 Kristiansand, Norway

*tor.inge.waag@teknova.no*

## ABSTRACT

This paper investigates the application of heterodyned Acoustic Emission (AE) compared to more conventional vibration measurements for Condition Monitoring (CM) of an offshore drilling machine, with a particular focus on the large, axial tapered roller bearing supporting the drill string weight in a top drive. The focus on cost reduction and operational uptime in the oil and gas industry motivates research on improved CM methods for fault detection, identification and ultimately prediction. However, bearing failure on this type of machines are currently responsible for a significant share of operational downtime on drilling rigs. In the experiment, a previously used and replaced bearing is compared to a new, healthy bearing with the purpose of identifying possible condition indicators (CI) from the vibration and AE measurements. AE root-mean-square values (RMS) was identified as a CI, being more consistent with the expected bearing health than vibration measurements and also less affected by operating speed. The AE measurements also show complementary forced frequency identification capabilities compared to the vibration measurements. The particular failure mode with bearing roller end damage is described and seen in conjunction with the results.

## 1. INTRODUCTION

The Rolling Element Bearing (REB) is a component found in basically all rotating machinery. It is also a common cause of premature machine failure. As bearings get larger, the consequence of failure typically increases in terms of unplanned

downtime cost and potential safety hazards. Simultaneously, maintenance actions are time-consuming, expensive and sometimes impossible to do on-site. The oil and gas industry is moving towards condition based maintenance strategies which require reliable CM methods. For the case of drilling machines, CM of the main bearing has proven to be difficult. A study of downtime causes on drilling rigs, the drilling machine was shown to be responsible for 13 % of downtime, with the bearing as the largest cause of failure (Jeffrey, 2012). The current industry standard is mainly a combination of visual inspection, periodic offline vibration measurements, and lubricant analysis. The statistics show an obvious potential for improvement, motivating the development of methods suitable for online CM of the bearing. This experiment is a rare opportunity to do measurements on a real drilling machine with a known damage to the bearing. The goal is to identify condition indicators for the main bearing and compare vibration measurements with AE measurements with regards to fault detection and identification.

Vibration analysis using accelerometers is the current industry standard for bearing CM, and has been researched for decades. Piezoelectric transducers are common for bearing CM, but MEMS-type accelerometers are also in use (Bechhoefer, Schlanbusch, & Waag, 2016). Likewise, the application of AE for bearing fault detection is not new in the field of CM of REBs, with early work done by (Yoshioka & Fujiwara, 1982, 1984). Heterodyning of the AE signal before sampling can be done to reduce the amount of stored and analyzed data for AE measurements, but maintain diagnostics information (Hecke, Yoon, & He, 2016). This reduction in data volume makes the technology more accessible for the industry, and is utilized in the experiment. AE measurements has also been combined with self-learning neural networks

---

Martin Hemmer et al. This is an open-access article distributed under the terms of the Creative Commons Attribution 3.0 United States License, which permits unrestricted use, distribution, and reproduction in any medium, provided the original author and source are credited.

(He, He, & Bechhoefer, 2016), which can further automate the analysis process.

The majority of research on bearing CM focus on signal processing methods for analysis of the time-waveform output by transducers. An extensive, categorized review of methods for bearing fault detection was presented by (Randall & Antoni, 2011). A recent advance is the development of cyclic spectral analysis, with notable work by (Antoni, 2007a, 2009). Cyclic spectral analysis can be applied to AE as well as vibration signals (Kilundu, Chimentin, Duez, & Mba, 2011).

Detection and diagnostics of discrete bearing faults are typically done by detecting the presence of one or more fundamental fault frequency; Ball Pass Frequency Inner Race (BPF<sub>I</sub>), Ball Pass Frequency Outer Race (BPF<sub>O</sub>), Cage Pass Frequency (CPF) and Ball Spin Frequency (BSF). However, to the authors' knowledge, CM methods specific for the failure mode described in this paper has not been thoroughly researched, opening new possibilities for future work in the field.

## 2. METHODS

This section describes the experimental setup, data acquisition systems, and data processing methods used to obtain the presented results.

### 2.1. Experimental Setup

Tests were performed on a large drilling machine taken out of operation for onshore maintenance. The main point of interest is the axial bearing, which normally supports the weight of the drillstring. The idea was to apply different systems to a relevant industrial application to compare performance. The machine already has measurement points for the radial and axial direction of the shaft, as shown in Figure 1. In this experiment, the only axial load on the bearing is caused by the shaft self-weight. The rotating motion is powered by a single hydraulic motor, connected to the shaft by a spur gear with a 8:1 ratio. Normally the machine uses up to four motors, but as the torsional load is low, only one motor was installed for this experiment. A pump for lubricant circulation is mounted to the side of the machine.

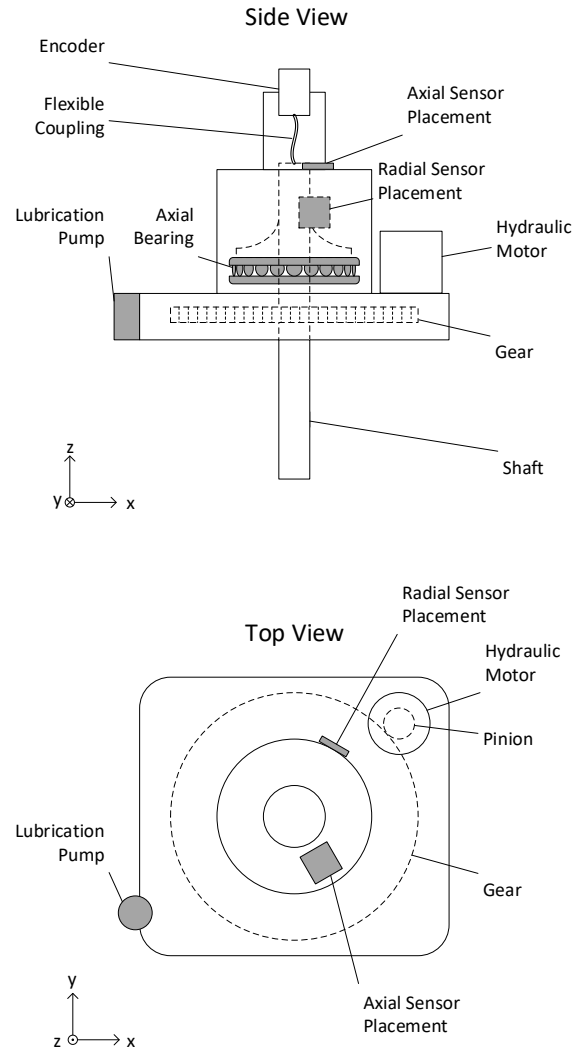


Figure 1. Experimental setup

### 2.2. Test Parameters

The experiment had two variable parameters; rotational speed and three stages of declining bearing condition. The three stages of declining bearing condition are termed Health Level (HL), with an index from 0 to 2. First, the machine was tested using a new, healthy bearing. This is referred to as HL0. HL1 refers to a previously used bearing, which was replaced due to observed roller end damage, described in section 3. The same bearing was subject to artificially created indentations on a roller end and run under poorer lubrication conditions to produce HL2. Basic test parameters including the main bearing fault frequencies is shown in Table 1. The fault frequencies are given in orders, with the main shaft as 1X. For each health level, the machine was tested at 5 rotational speeds ranging from 50 RPM (0.83 Hz) to 250 RPM (4.17 Hz). The main bearing was not subject to external axial load except shaft

self-weight. The bearing load of 9.83 kN is significantly less than typical load under operation, further complicating fault detection.

Table 1. Bearing Operating Information

Test Information	
Bearing diameter	650 mm
Bearing load	9.83 kN
Test speeds, [RPM]	{50 – 100 – 150 – 200 – 250}
Test speeds, [Hz]	{0.83 – 1.67 – 2.5 – 3.34 – 4.17}
Main shaft speed	1X
Motor shaft speed	8X
BPFI	8.68X
BPFO	8.32X
BSF	6.75X
CPF	0.49X

### 2.3. Sensor Placement

The drilling machine is equipped with measurement points for routine CM. However, to accommodate several transducers logging simultaneously, an adapter plate was made from a 20mm steel plate. The sensors were placed on a circle centered on the mounting flange to make the signal transmission path as equal as possible.

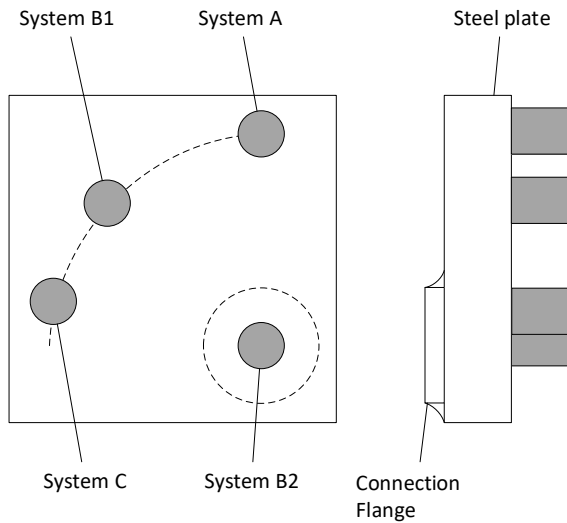


Figure 2. Sensor placement on adapter plate

### 2.4. Instrumentation

Data acquisition was done using 3 different systems, two of which utilizes acceleration transducers while the third one uses an AE transducer. The benchmark for acquisition time was a frequency resolution of 10-30 bins between fault frequencies, as recommended in (Bechhoefer et al., 2016). System A recorded for 100 revolutions regardless of rotational speed while the other systems sampled fixed length time series. Key specifications are given in Table 2.

Table 2. Instrumentation

Feature	System A	System B	System C
Transducer	Acceleration	Acceleration	AE
Frequency	2 Hz -10 kHz	2 Hz -10 kHz	50-400 kHz
Sensitivity	10 $mV/ms^{-2}$	1.0 $\mu A/ms^{-2}$	69 dB (peak)
Sample rate	102.4 kHz	10 kHz	50 kHz
Recording	100 rev	60 s	120 s

#### 2.4.1. System A

System A consists of a piezoelectric accelerometer with a sensitivity of 100 mV/g and linear range of 2 Hz to 10 kHz. However, with a sampling rate of 102.4 kHz, the signal is oversampled compared to the linear range. This was done to capture encoder data, which was logged simultaneously on the same system to allow RPM calculation and order tracking.

#### 2.4.2. System B

System B is part of a commercially available CM system, using an Integrated Electronics Piezoelectric Accelerometer with a current output sensitivity of 1.0  $\mu A/ms^{-2}$ . For the purpose of this paper, the time-waveform is extracted and analyzed to ensure control of signal processing methods used. Sampling is limited to 10 kHz for 60 seconds. The system is installed at two locations, named B1 and B2 for distinction, shown in Figure 2. System B2 is mounted directly over the connection flange, where the accelerometer is normally mounted, to serve as a reference measurement.

#### 2.4.3. System C

System C uses an AE transducer glued to the measurement surface. The frequency range is 50 to 400 kHz. However, the signal is heterodyned and demodulated by an analog circuit before sampling, which allows the sampling frequency of 50 kHz. The preprocessing method applied to AE signals was presented in (Qu, Bechhoefer, He, & Zhu, 2013). The high frequency heterodyne product is filtered out, and the low frequency is phase-shifted by  $\frac{\pi}{2}$ , which effectively is the

complex part of the Hilbert transform of the signal. Sampling both the original signal and the phase-shifted version allows demodulation simply by calculating the absolute value of the two.

### 3. FAILURE MODE

The bearing is a pure axial tapered roller bearing, supporting the drillstring. The rollers are tapered to maintain rolling line contact between roller and races during rotation. A retaining flange is necessary to keep the rollers in place due to the wedge effect of the tapered roller. Simplified, the forces acting on the roller is shown in Figure 3. The axial load  $F_A$  is decomposed in two components;  $F_N$  normal to the tapered bearing raceway, and  $F_C$  acting on the roller end towards the roller apex point. The relative magnitude of  $F_N$  and  $F_C$  depends on the cone angle  $\beta$ . Due to the inevitable sliding contact at the roller end, this area is exposed to surface wear. This corresponds well with the observed damage on the worn bearing in the drilling machine, which initiated the maintenance action.

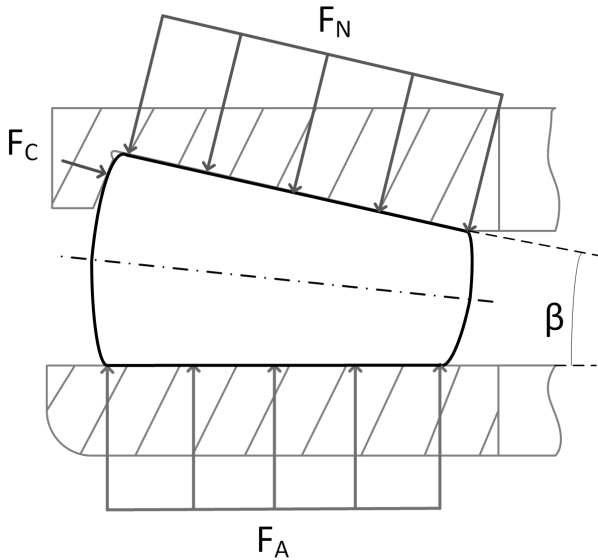


Figure 3. Internal bearing forces

Arc-shaped scratches with varying radius are observed across the roller end surface, as shown in Figure 4. Generation of such damage can be explained by observing the trace of a particle stuck on the retaining flange, which is passed by a roller. Figure 5 shows this trace for 3 particles at different distances from the rolling surface.

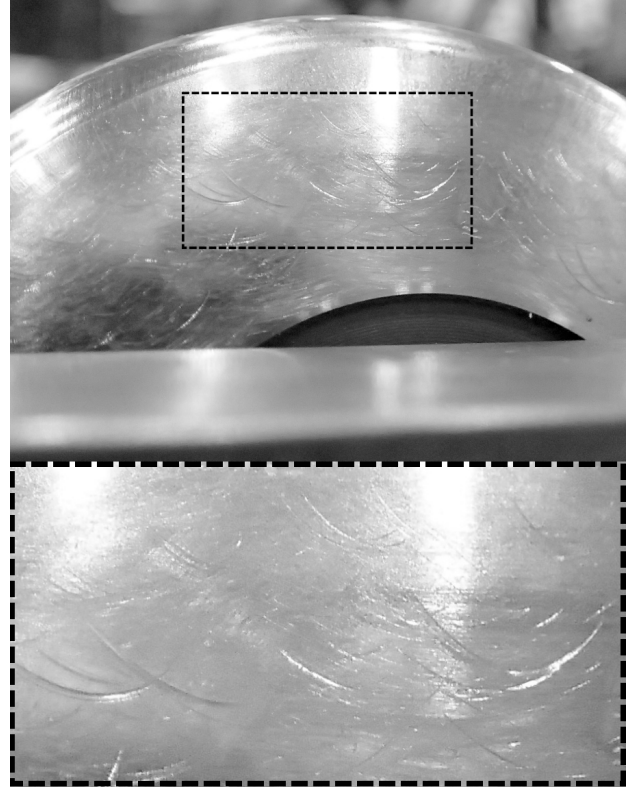


Figure 4. Characteristic roller end damage

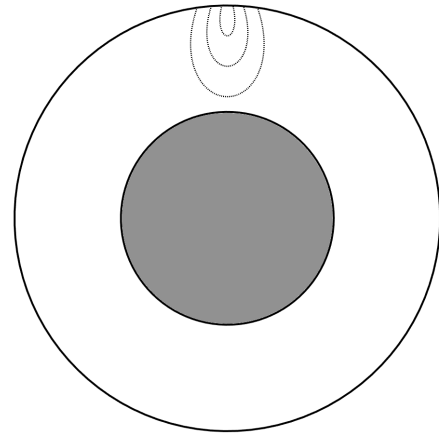


Figure 5. Trace of particles on a roller end

The distribution of scratches appears to be relatively even between rollers. As it is not a clear, discrete fault, an assumption of periodic behavior may be invalid, which makes traditional frequency analysis tools less useful. Generation of scratches implies permanent changes in the metallic structure, which will generate an AE transient. Also, as the number of scratches increases, the accumulated amount of particles in the lubricant should grow at an increasing rate, leading to a similar growth in scratch formation and AE activity.

**4. RESULTS**

The presented results highlight observed differences between the vibration and AE measurement system for overall value trending and feature detection in the frequency domain.

**4.1. RMS Trending**

A change in signal RMS values can be used to indicate a change in condition. In this experiment, there was a known change component health, which was expected to cause an increase in RMS. Measurements from system B2 show an increase in RMS with RPM for all HLs, shown in Figure 6. However, from HL0 to HL1, the RMS decrease unexpectedly, and remains low at HL2. The same trend occurs in data from systems A and B1, shown in Table 3. The levels for system B2 are generally higher than for B1 in the axial direction and lower in radial direction. Sensor placement is the only difference between systems B1 and B2, indicating that the adapter plate transfer function has an effect on the measurements. System B2 has the shortest signal transmission path and the stiffest connection, which should produce the most accurate results.

Interestingly, results from the AE measurements (system C) show a different trend. As shown in Figure 7 and Table 3, there is an increase in AE RMS at HL1 and HL2. At HL1, radial RMS values increase with a factor of 1.5-2.2, whereas axial RMS increase by a maximum factor of 1.2 at 250 RPM. At HL2 the increase is distinct in both directions, with a relative increase from HL0 of 5.1 and 4.2 for radial and axial RMS respectively. The radial measurement point, shown in Figure 1, is located closer to the bearing. The longer signal transmission path can explain the higher AE RMS levels, assuming that the bearing is a source of AE activity. The AE RMS increases with RPM, but less than the corresponding vibration measurements. For an increase in RPM from 50 to 250 RPM, System A and B RMS increase by a factor in the range from 2.6 to 12.9, while for system C the range is 1.6 to 2.3.

The power spectrum of the AE signal is shown for 150 RPM in Figure 8. The reveals an overall, broadband increase in activity. The power spectrum  $P(f)$  is calculated as shown in Equation 1, simply by applying the Fast Fourier Transform, denoted  $FFT\{\cdot\}$  to the squared signal. Peaks in the spectrum can not be related to the bearing fault frequencies, but is addressed in section 4.2.

$$P(f) = FFT\{|x(t)|^2\} \tag{1}$$

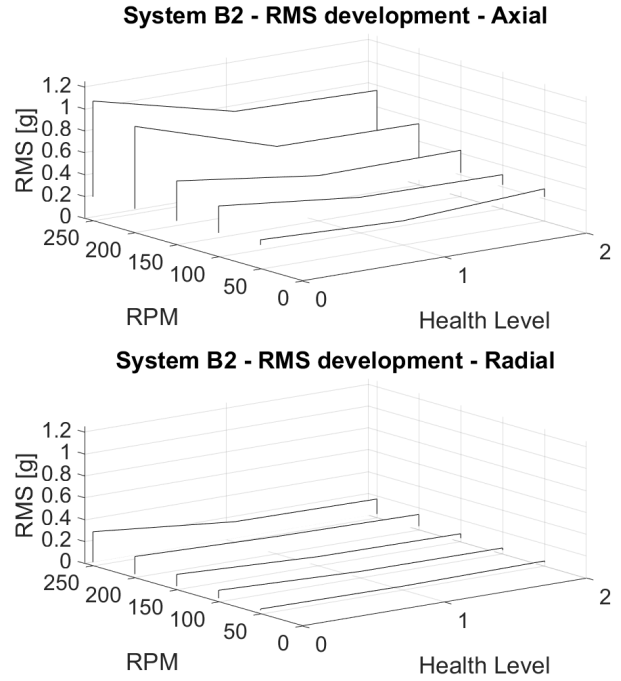


Figure 6. RMS trend for system B2

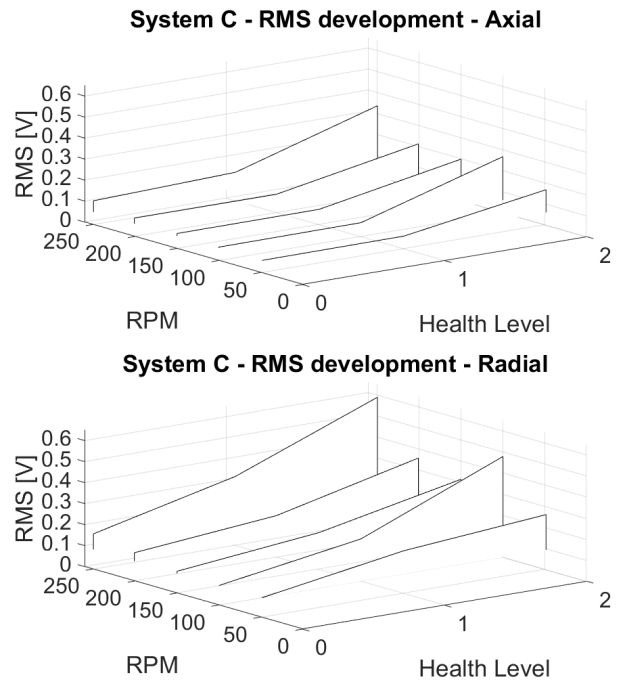


Figure 7. RMS trend for system C

Table 3. RMS Values

Acceleration RMS-value [ $10^{-3}$ g]											
	RPM	Axial					Radial				
		50	100	150	200	250	50	100	150	200	250
System A	HL 0	11.5	30.9	40.0	59.9	85.7	15.7	32.5	46.8	44.6	99.8
	HL 1	12.2	17.1	28.0	36.0	46.0	8.0	13.0	19.8	31.7	41.5
	HL 2	11.6	15.3	23.6	29.3	39.0	9.9	14.1	17.9	33.0	33.7
System B1	HL 0	96.6	256.7	352.8	764.1	819.3	83.2	216.9	278.7	479.5	1069.3
	HL 1	74.8	136.4	183.9	316.7	390.7	81.0	156.9	237.0	461.7	521.0
	HL 2	94.8	146.6	212.4	416.6	438.2	111.1	159.8	207.4	364.3	541.0
System B2	HL 0	266.9	466.0	584.8	973.0	1094.5	45.6	106.5	142.1	195.1	311.7
	HL 1	219.5	325.7	413.2	570.1	780.6	33.8	59.7	85.1	158.9	183.5
	HL 2	293.6	312.5	425.4	558.1	752.6	45.4	54.1	74.1	140.6	171.3
AE RMS-value [ $10^{-3}$ V]											
System C	HL 0	59,9	64,2	71,9	87,0	113,3	94,5	93,6	104,2	134,0	168,1
	HL 1	61,4	66,1	72,6	85,9	135,0	203,9	201,2	174,2	196,4	327,4
	HL 2	167,8	266,2	197,4	211,6	337,4	261,2	479,2	313,7	356,2	589,8

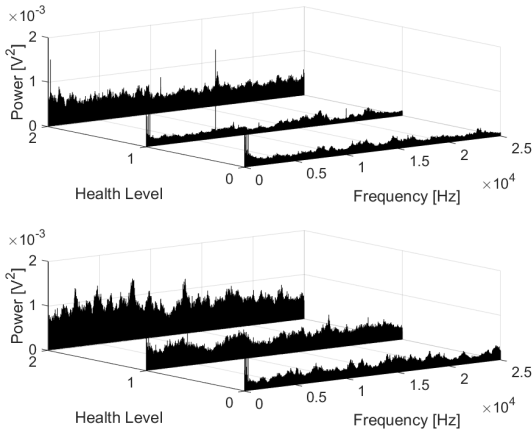


Figure 8. System C power spectrums at 150 RPM

#### 4.2. Forcing Frequency Identification

The processing of recorded data did not reveal any clear indications of faults on component level. Still, the systems show differences in the ability to identify forcing frequencies. Figure 9 and 10 show the envelope power spectrum from HL2 at 150 RPM, using data from system A and C, respectively. 1X and 8X harmonics with 1X sidebands dominates the spectrum from vibration measurements, shown in Figure 9. However, one particular, non-synchronous feature was detected in 14 of 15 AE measurements. Table 4 shows the peak frequency at the different operating speeds and health levels.

Table 4. Identified pump frequencies

Health Level	0	1	2
RPM	Observed Frequency [Hz]		
50	17.24	16.71	18.91
100	17.30	16.78	16.9
150	17.34	17.04	18.87
200	17.38	17.19	18.76
250	17.47	-	17.1

The peak appeared at similar frequencies regardless of operating speed. The source of this frequency is assumed to be a small lubrication pump located on the side of the machine, shown in Figure 1, approximately 1 meter from the measurement point. Completely uncoupled from the main shaft, it was identified as the only component rotating in the detected frequency range.

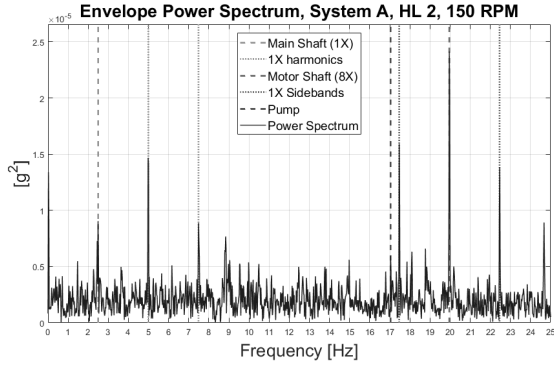


Figure 9. System A envelope power spectrum

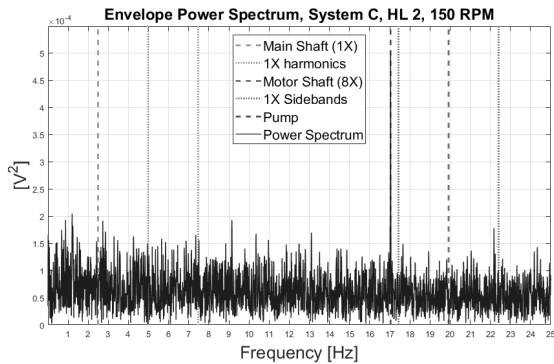


Figure 10. System C envelope power spectrum

Computation of the fast kurtogram, as described in (Antoni, 2007b), was used to identify frequency bands with elevated kurtosis. However, no clear improvement in forcing frequency identification was observed. The results shown in table 4 are calculated for the top level of the kurtogram, which corresponds to low-pass filtering up to the Nyquist frequency before calculating the envelope. For the vibration measurements, the envelope power spectrum is calculated from the square of time-waveform  $x$ . The envelope is then the absolute value of the analytic signal, computed using the Hilbert transform, denoted  $H\{\cdot\}$ , as shown in Equation 2.

$$Envelope = |x(t)^2 + jH\{x(t)^2\}| \quad (2)$$

For the AE measurements, an approximation of the analytic signal is created by analog pre-processing as described in section 2.4.

## 5. DISCUSSION AND CONCLUSION

In this paper, 3 different CM systems utilizing accelerometer and AE transducers have been applied to an offshore drilling machine. A healthy bearing was used as reference for a worn bearing, which then was tested at two stages of declining health.

Despite low utilization of the axial load capacity, it was possible to detect an increase in RMS of the AE signal that corresponds to the change in bearing health. The fact that vibration measurement systems gave higher RMS values for the healthy bearing simply highlights the need for comparable operating conditions when trending. The process of replacing the healthy bearings with the used one, implied complete disassembly of the machine, effectively changing the basis of comparison. The consistent increase in AE RMS makes this CI more promising. AE RMS measurements were also less affected by rotational speed, which is an advantage for machines under varying operating conditions. AE measurements also showed an ability to detect some modulation frequencies not visible in the acceleration spectrum. In particular, a frequency which is assumed to be a lubrication pump was detected, in spite of a long signal transmission path. In the authors' opinion, this illustrates that measurement systems using AE transducers can complement vibration based systems.

The observed failure mode lacks a dominant localized fault, which results in a lack of periodic impacts. Hence, methods based on detection of bearing fundamental frequencies were ineffective. Artificially induced indentations were applied to a roller end, but a roller fault could not be identified from the measurements. Due to low utilization of bearing load capacity, the bearing is less prone to breakage of the oil film on the roller ends, which is a requirement for detection of roller end damage. While the overall increase in AE activity still corresponded to declining bearing health, it is unlikely that the increase is due to formation of new scratches. The results support AE as a CM technology for axial tapered roller bearings in drilling machines and other rotating machinery. The shown fault frequency identification capabilities combined with possible detection of scratch formation on roller ends motivates further research on the topic, in particular to capture and identify the failure mode propagation.

## ACKNOWLEDGMENT

The research presented in this paper has received funding from the Norwegian Research Council, SFI Offshore Mechanics, project number 237896.

## REFERENCES

- Antoni, J. (2007a). Cyclic spectral analysis of rolling-element bearing signals: Facts and fictions. *Journal of Sound and Vibration*, 304(3-5), 497–529. doi: 10.1016/j.jsv.2007.02.029
- Antoni, J. (2007b). Fast computation of the kurtogram for the detection of transient faults. *Mechanical*

- Systems and Signal Processing*, 21, 108–124. doi: 10.1016/j.ymssp.2005.12.002
- Antoni, J. (2009). *Cyclostationarity by examples* (Vol. 23) (No. 4). doi: 10.1016/j.ymssp.2008.10.010
- Bechhoefer, E., Schlanbusch, R., & Waag, T. I. (2016). Techniques for Large, Slow Bearing Fault Detection. *International Journal of Prognostics and Health Management*, 7(1), 1–12.
- He, M., He, D., & Bechhoefer, E. (2016). Using Deep Learning Based Approaches for Bearing Fault Diagnosis with AE Sensors. In *Annual conference of the prognostics and health management society* (pp. 1–10).
- Hecke, B. V., Yoon, J., & He, D. (2016). Low speed bearing fault diagnosis using acoustic emission sensors. *APPLIED ACOUSTICS*, 105, 35–44. doi: 10.1016/j.apacoust.2015.10.028
- Jeffrey, L. (2012). *Noble 2012 Analyst & Investor Day presentation*.
- Kilundu, B., Chiementin, X., Duez, J., & Mba, D. (2011). Cyclostationarity of Acoustic Emissions (AE) for monitoring bearing defects. *Mechanical Systems and Signal Processing*, 2061–2072. doi: 10.1016/j.ymssp.2011.01.020
- Qu, Y., Bechhoefer, E., He, D., & Zhu, J. (2013). A New Acoustic Emission Sensor Based Gear Fault Detection Approach. *International Journal of Prognostics and Health Management*, 4, 1–14.
- Randall, R. B., & Antoni, J. (2011). Rolling element bearing diagnostics-A tutorial. *Mechanical Systems and Signal Processing*, 25(2), 485–520. doi: 10.1016/j.ymssp.2010.07.017
- Yoshioka, T., & Fujiwara, T. (1982). A new acoustic emission source locating system for the study of rolling contact fatigue. *Wear*, 81(1), 183–186.
- Yoshioka, T., & Fujiwara, T. (1984). Application of acoustic emission technique to detection of rolling bearing failure. *American society of mechanical engineers*, 14(1), 55–76.